

See discussions, stats, and author profiles for this publication at: <https://www.researchgate.net/publication/231644430>

# Enhanced Catalytic Activity of Carbon Alloy Catalysts Codoped with Boron and Nitrogen for Oxygen Reduction Reaction

ARTICLE *in* THE JOURNAL OF PHYSICAL CHEMISTRY C · APRIL 2010

Impact Factor: 4.77 · DOI: 10.1021/jp100045e

---

CITATIONS

31

READS

42

## 7 AUTHORS, INCLUDING:



**Mauro Boero**

Institut de Physique et Chimie des Matéria...

187 PUBLICATIONS 3,479 CITATIONS

[SEE PROFILE](#)



**K. Terakura**

National Institute of Advanced Industrial S...

374 PUBLICATIONS 13,151 CITATIONS

[SEE PROFILE](#)

# Enhanced Catalytic Activity of Carbon Alloy Catalysts Codoped with Boron and Nitrogen for Oxygen Reduction Reaction

Takashi Ikeda,<sup>\*,†</sup> Mauro Boero,<sup>‡,§</sup> Sheng-Feng Huang,<sup>‡</sup> Kiyoyuki Terakura,<sup>‡,||</sup>  
Masaharu Oshima,<sup>†</sup> Jun-ichi Ozaki,<sup>#,||</sup> and Seizo Miyata<sup>||</sup>

Synchrotron Radiation Research Unit, Quantum Beam Science Directorate, Japan Atomic Energy Agency (JAEA), Hyogo 679-5148, Japan, Research Center for Integrated Science, Japan Advanced Institute of Science and Technology (JAIST), 1-1 Asahidai, Nomi, Ishikawa 923-1292, Japan, Institut de Physique et Chimie des Matériaux de Strasbourg, UMR 7504 CNRS-UdS, 23 rue du Loess, 67034 Strasbourg, France, Department of Organic and Polymeric Materials, Graduate School of Science and Engineering, Tokyo Institute of Technology, 2-12-1 S5-20, Ookayama, Tokyo 152-8552, Japan, Department of Applied Chemistry, The University of Tokyo, 7-3-1 Bunkyo-ku, Tokyo 113-8656, Japan, and Department of Chemical and Environmental Engineering, Graduate School of Engineering, Gunma University, 1-5-1, Tenjin-cho, Kiryu, Gunma 376-8515, Japan

Received: January 4, 2010; Revised Manuscript Received: April 13, 2010

Carbon alloy catalysts (CACs) have been attracting a growing interest as potential Pt-free electrode catalysts for polymer electrolyte fuel cells. In this computational study, we inspect possible oxygen adsorption and reduction processes on various models for exposed edges of these catalysts via first-principles molecular dynamics. Our simulations suggest that the codoping of boron and nitrogen in CACs is a promising route to the further enhancement of their catalytic activity with respect to both stability and reactivity.

## Introduction

The polymer electrolyte fuel cell (PEFC) is likely to become one of the most promising power sources in the near future because of its rather high efficiency, low operating temperature, no or little environmental drawbacks, etc. However, its practical use is still hindered by the prohibitive cost of Pt-based catalysts required for electrode reactions at operating temperatures around 80 °C. In an attempt at reducing the cost of PEFCs, several researchers have tried developing alternative Pt-free electrode catalysts using more abundant elements. Because the rate of the oxygen reduction reaction (ORR) at the cathode is significantly lower than that of the counterpart hydrogen oxidation reaction at the anode, research efforts target mainly the cathode.

Recently, several groups<sup>1–7</sup> reported surprisingly high ORR activity in carbon-based nanomaterials doped with N (and B). Such carbon-based materials, including a certain amount of heteroatoms, are termed carbon alloys.<sup>8</sup> In parallel with traditional semiconductor technologies, a systematic study of carbon alloys is expected to enable the realization of high-performing materials. In fact, the materials synthesized via carbonization processes of carbon polymers and nitrogen precursors, such as, for instance, phthalocyanine, exhibit some remarkable features. First, they are constituted by a substantial amount of nanoshells mainly composed of  $sp^2$  carbon. Second, the ORR activity is significantly enhanced by increasing the concentration of N (or by codoping of B and N). Furthermore, the presence of defects, detected by transmission electron microscopy (although still unidentified at atomic scale), is likely to contribute, at least partly, to the high ORR activity. These findings indicate that

carbon alloy catalysts (CACs) are likely to possess a catalytic activity comparable to conventional Pt-based catalysts.

A rational design and tuning of their catalytic performance require primarily a detailed atomistic insight into the arrangement of dopants in the carbon network. This information cannot be easily extracted from experiments because CACs have a complex structure and reaction intermediates are generally too short-lived to be detected. Nonetheless, soft X-ray absorption spectroscopy (XAS) measurements, aimed at investigating the electronic states originating from the N-doping in CACs, showed three peaks in the  $\pi^*$  region of N 1s XAS.<sup>9</sup> This indicates that N occupies at least three chemically different sites. The variation of the relative intensity of these three peaks was found to be correlated with the relative ORR activities of the samples differing in the N-doping method. More active samples contain more graphite-like rather than pyridine-like N, suggesting a close relationship between 3-fold N and ORR activity.

In our previous study,<sup>10</sup> possible adsorption states and subsequent reduction steps of  $O_2$  on N-doped CACs were explored via first-principles molecular dynamics (MD) and showed that specific N sites enhance the catalytic activity without requiring metal catalysts. Moreover, a recent advancement in our computational study<sup>11</sup> has revealed that these particular N-dopant configurations, able to enhance the catalytic activity, are less stable than other configurations potentially responsible for suppression rather than enhancement of the activity. Therefore, we must remark that CACs synthesized for practical use would somehow satisfy two apparently incompatible requirements of stability and reactivity. In this work, we show that the above difficulties can, in principle, be partly reconciled by the codoping of boron and nitrogen, thus allowing for an enhancement of the activity of CACs without involving unstable dopant structures.

## Computational Method

The oxygen adsorption and subsequent reduction processes were investigated as described in our previous paper.<sup>10</sup> Specif-

\* To whom correspondence should be addressed. E-mail: ikeda.takashi@jaea.go.jp.

† Japan Atomic Energy Agency (JAEA).

‡ Japan Advanced Institute of Science and Technology (JAIST).

§ IPCMS.

|| Tokyo Institute of Technology.

† The University of Tokyo.

# Gunma University.

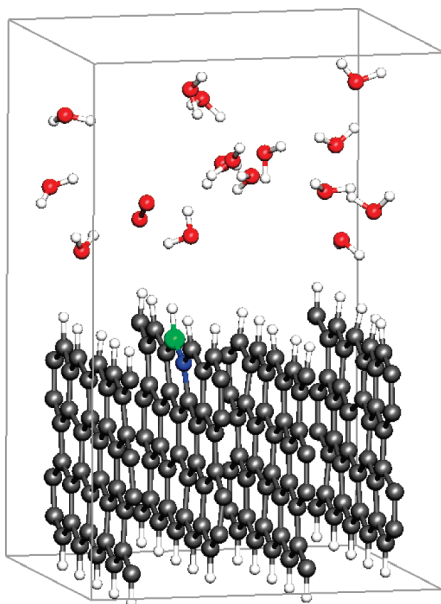


**Figure 1.** Example of our model systems consisting of 4 graphene sheets, an  $O_2$  molecule, and 15  $H_2O$  molecules. The simulation box of  $12.278 \times 20.000 \times 13.392 \text{ \AA}^3$  is shown as gray lines. Atom colors are white for H, gray for C, green for B, blue for N, and red for O.

ically, our simulations are based on a Car–Parrinello MD approach,<sup>12,13</sup> within a plane-wave pseudopotential framework for the density functional theory (DFT), including Hamprecht–Cohen–Tozer–Handy (HCTH) gradient corrections<sup>14</sup> on the exchange and correlation functionals in an unrestricted-spin scheme. The performance of this particular functional for liquid water and solution systems has already been investigated and assessed in previous studies.<sup>15–20</sup> The valence–core interaction was described by Troullier–Martins<sup>21</sup> pseudopotentials (PPs) for B, C, N, and O and a von Barth–Car<sup>22</sup> PP for H. The sampling of the Brillouin zone was restricted to the  $\Gamma$  point. A systematic set of simulations was performed for various slab models composed of graphene sheets doped with B or N or both dopants at different positions, one  $O_2$  molecule, and a certain amount of  $H_2O$  molecules in a simulation box with periodic boundary conditions, as displayed in Figure 1. Our systems thus amount to about 200 atoms, consisting of two (for basal plane) or four (for edge plane) graphene sheets with bottom C fixed to bulk graphite and saturated with H, and a water layer ( $\sim 10 \text{ \AA}$ ) plus an  $O_2$  molecule initially in a spin-triplet state. The borders of the graphene sheets far from the catalytic center were restrained to oscillate around the crystal positions by a harmonic potential to mimic the environment around a hypothetical CAC cathode in PEFCs. Although our systems are likely to be oversimplified,<sup>23</sup> the system size has to be reduced to several hundreds of atoms to make computations feasible at an acceptable cost. Free-energy barriers for the adsorption and subsequent reduction of  $O_2$  were estimated by the blue moon ensemble method<sup>18,24–26</sup> whenever necessary. The accuracy of the free-energy estimations is, at very best,  $\sim 1 \text{ kcal/mol}$ , which is a typical error bar of any present-day DFT approach.<sup>27</sup> The temperature was kept at 300 K by velocity rescaling throughout the present study.

## Results and Discussion

**Oxygen Adsorption.** To examine possible  $O_2$  adsorption sites in CACs, we prepared eight different model structures to reproduce three possible configurations of basal plane, zigzag-

edged plane, and zigzag-shaped step edge on the exposed surface, as shown in Figure 2, where some  $sp^2$  C atoms were replaced with B or N. These models were interfaced with a 10  $\text{\AA}$  dilute water layer, including an  $O_2$  molecule initially in its ground state (triplet) far from the surface. Free-energy barriers for adsorption of an  $O_2$  molecule were then computed by decreasing the distance of this  $O_2$  from the adsorption sites. For each point, we performed blue moon ensemble simulations for at least 1.0 ps to re-equilibrate the system. We remark that all the free-energy barriers were estimated at a fixed total  $S_z$ , thus allowing  $O_2$  to change its spin state as a result of the interaction with the adsorbents.

According to our analysis of the relative stability of various dopant configurations for a graphene cluster, pyridinium-like N (Figure 2a) and boratabenzene-like B (Figure 2b) correspond to the most stable configurations among the possible single-N and single-B dopants, respectively. The computed free-energy differences  $\Delta F$  for  $O_2$  adsorption on these stable dopant sites represent qualitatively different behaviors, as shown by curves a and b in Figure 3. By decreasing the distance  $d_{\#-O_2}$  between  $O_2$  and the target site labeled as # (# = a, b, c-1, c-2, d, e, f, g, and h and marked with arrows in Figure 2), the free-energy profile for pyridinium-like N exhibits a monotonic increase, whereas for boratabenzene-like B,  $\Delta F$  has a minimum at  $d_{\#-O_2} \sim 1.9 \text{ \AA}$  after taking a maximum at  $\sim 2.6 \text{ \AA}$ , although the adsorbed  $O_2$  is not characterized by a high stability. On the other hand, as reported in ref 10,  $\Delta F$  for a substitutional N next to the zigzag edge shows a maximum at  $d_{\#-O_2} \sim 2.3 \text{ \AA}$  and, subsequently,  $O_2$  molecules become tightly bound to C atoms at zigzag edges. However, the relative total energy for such a graphite-like N is found to be about 1.0 eV higher than that for a pyridinium-like N, indicating that relevant configurations suited to promote ORR activity are hardly realized from a thermodynamic point of view if a single type of dopant is employed. Interestingly, strong attractive interatomic interaction acting between neighboring B and N atoms works very effectively to reduce the difference of the relative total energies down to about 0.4 eV for the next lowest configurations (Figure 2c,d) of a B–N pair doped at zigzag edges with respect to the corresponding lowest ones (Figure 2f,g).<sup>11</sup> Moreover, free-energy barriers for  $O_2$  adsorption are remarkably lowered, particularly for the zigzag-edged plane (curve c-2) and zigzag-shaped step edge (curve d), by changing the target site from edge C to dopant B sites, as shown in Figure 3. Furthermore, for case f of the most stable B–N pair configurations (curve f of Figure 3),  $\Delta F$  approaches the one for pure zigzag edges without dopants. A high chemical reactivity of zigzag edges of pure graphene was already suggested in former studies of refs 10 and 28. Even for the case labeled as g (Figure 3), where  $O_2$  approaches the edge C in the opposite side of the B–N pair to the case f,  $\Delta F$  shows a much more moderate increase compared with the case of pyridinium-like N in the absence of B dopants. These results indicate that a negative effect of pyridinic N on the  $O_2$  adsorption is partly compensated by a B–N codoping. Note that the presence of B–N pairs in the basal plane does not give rise to stable adsorption structures of  $O_2$  molecules, as demonstrated by curve e of Figure 3. By considering the van der Waals correction in the Grimme’s empirical scheme,<sup>29</sup> the free-energy profile at room temperature is found to show a deviation from curve e of Figure 3, which is, however, still within the expected computational accuracy of  $\sim 2 \text{ kcal/mol}$ . Hence, our simulations suggest that edge localized states near the Fermi level that are specific to zigzag edges play a crucial role in the  $O_2$  adsorption. Relevant edge states are modified by

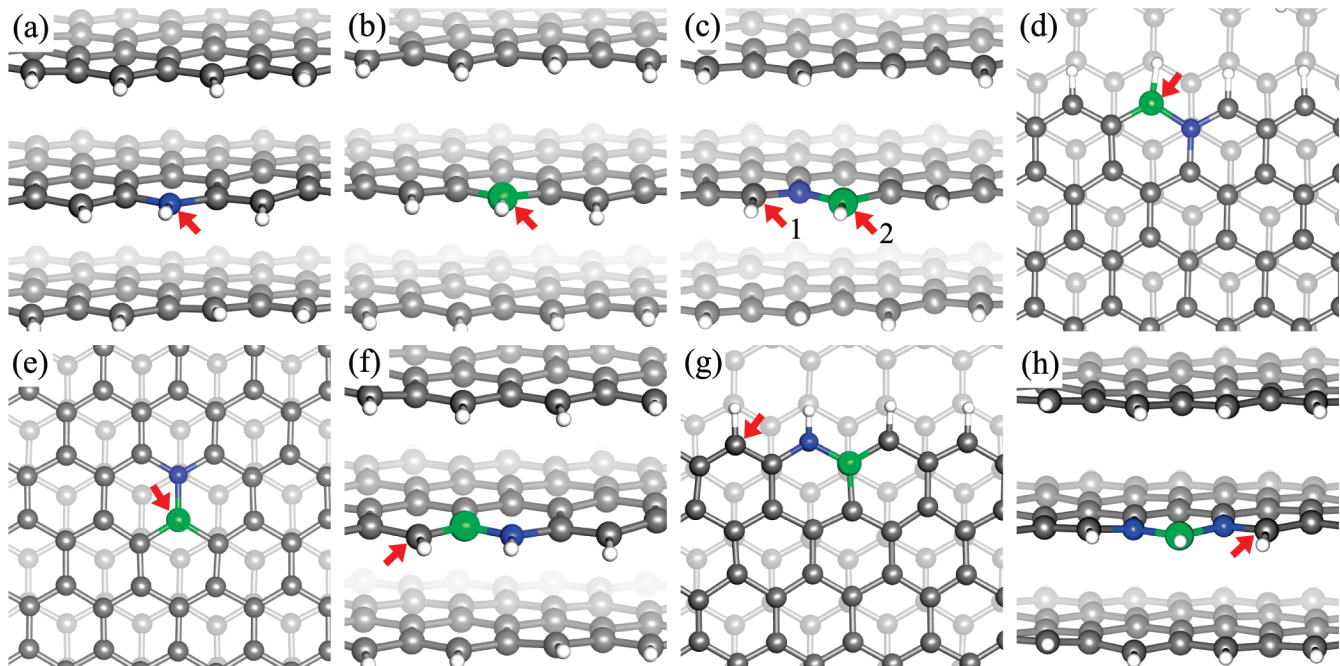


**Figure 2.** Model structures of CACs for  $O_2$  adsorption. The models a and b contain pyridinium-like N and boratabenzene-like B, respectively. A B–N pair is included at a zigzag-edged plane, zigzag-shaped step edge, and basal plane for models c–e, respectively. In models f and g, the positions of B and N are exchanged with respect to models c and d. Model h contains an N–B–N complex at a zigzag edge. Atom colors are white for H, gray for C, green for B, and blue for N. We estimated the free-energy profile for  $O_2$  adsorption by making an  $O_2$  molecule approach the target sites marked by arrows in each panel.

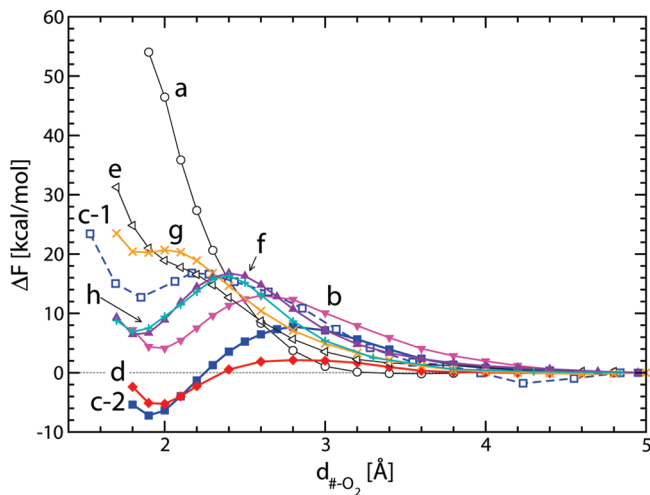


**Figure 3.** Free-energy profiles for  $O_2$  adsorption on atoms marked by arrows in Figure 2. The reaction coordinate is the distance between the center of mass of the  $O_2$  molecule and the expected adsorption site labeled as #, where # denotes a, b, c-1, c-2, d, e, f, g, and h.

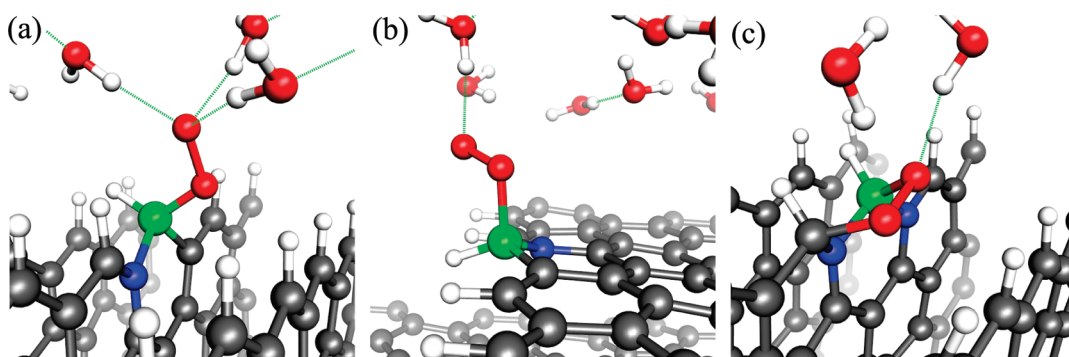
B and N codoped at zigzag edges so that  $O_2$  molecules are more easily converted to  $O_2^{\delta-}$  at around the transition state, thus promoting the  $O_2$  adsorption onto doped B atoms. Indeed, for a N–B–N complex at zigzag edges (Figure 2h), we observed that an  $O_2$  molecule is bound first to the dopant B site upon overcoming a free-energy barrier of 16 kcal/mol (curve h), even though an edge C is assumed to be the target site. More detailed discussion about the relationship between the modification of electronic structure by B-doping and the  $O_2$  adsorption will be given elsewhere.

Figure 4 shows typical structures of adsorbed  $O_2$  observed in our simulations for B–N-codoped CACs. We found that  $O_2$  molecules are adsorbed mostly on B atoms in the end-on configuration, while preserving one or more hydrogen bonds between the terminal O and  $H_2O$  molecules in its vicinity (Figure

4a,b). However, the side-on configuration is also almost equally possible for N–B–N-doped zigzag edges, as sketched in Figure 4c. We should note that B atoms located at zigzag edges in a B–N–C moiety always work as adsorption sites of  $O_2$  molecules. Thus, the amount of this type of B dopants included in B–N-doped CACs will have a simple (probably linear) relationship with the degree of catalytic activity.

**Oxygen Reduction.** The subsequent steps of  $O_2$  reduction were investigated, assuming that additional  $e^-$  and  $H^+$  are supplied separately and consecutively from the anode through an external circuit and a polymer electrolyte, respectively. In these simulations, we assumed the possible lowest total spin state according to the number of electrons in our system. Our inspection of the reduction processes was restricted to the two cases of an adsorbed  $O_2$  on the c-2 and d sites of Figure 2 because these two cases are characterized by remarkably lower free-energy barriers for  $O_2$  adsorption (see Figure 3). Note that, because the structure of the interface between cathode catalysts and water solutions could be much more complex in PEFCs, the proton-transfer process, which is expected to be a candidate for the rate-determining step of ORR, could not be well-reproduced in our simulations. Thus, our investigations were rather focused on the processes directly related to the catalysts.

We found that the ORR depends on the orientation of the exposed surface. For the zigzag-edged surface, two or three hydrogen bonds are formed between the terminal O of the –B–O–O adduct and  $H_2O$  molecules, as shown in Figure 4a. The middle O of the –B–O–O will not be solvated because of the hydrophobicity of the –CH groups of the substrate. Thus, a selective  $H^+$  attack to the terminal O occurs immediately once an additional  $H^+$  is supplied. The addition of two extra electrons and an extra proton then leads to the breaking of the O–O bond in the resulting –B–O–O–H adduct because additional electrons occupy the low-lying orbitals characterized by large O–O antibonding character, though our electronic structure calculations may suffer from common deficiencies of the present



**Figure 4.** Structure of adsorbed  $\text{O}_2$  on the B–N-doped (a) zigzag-edged surface and (b) zigzag-shaped step edge and (c) the N–B–N-doped zigzag-edged surface. Hydrogen bonds are indicated as dashed lines. H is white, C is gray, B is green, N is blue, and O is red.

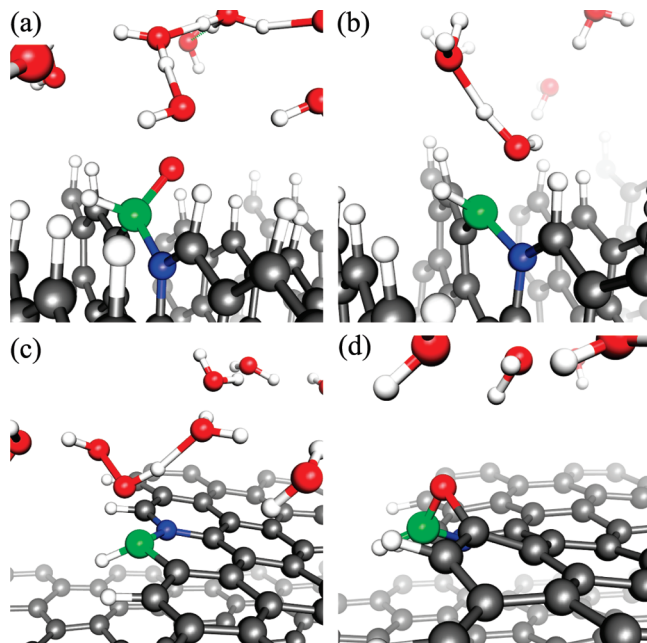


**Figure 5.** Reduction processes of an adsorbed  $\text{O}_2$  on B–N-doped CACs. Upper panels show the successive formation of  $\text{H}_2\text{O}$  molecules upon proton transfer to the adducts (a)  $-\text{B}-\text{O}-\text{O}-\text{H}$  and (b)  $-\text{B}-\text{O}-\text{H}$  on the zigzag-edged surface, whereas lower ones show the formation of (c) a  $\text{H}_2\text{O}_2$  and (d) a metastable intermediate upon proton transfer to the adduct  $-\text{B}-\text{O}-\text{O}-\text{H}$  on the step edge. H is white, C is gray, B is green, and N is blue.

standard DFT calculations, such as spin contamination, self-interaction error, etc., in the description of the  $\text{O}_2$  dissociation. Therefore, the formation of the first  $\text{H}_2\text{O}$  molecule occurs without requiring any appreciable activation energy (Figure 5a).

By adding other two protons and two electrons in the sequence of  $\text{H}^+$ ,  $\text{e}^-$ ,  $\text{H}^+$ , and  $\text{e}^-$ , the subsequent reduction of the remaining O atom on the adsorption site, which leads to the formation of a second  $\text{H}_2\text{O}$  (Figure 5b), was observed to proceed in a smooth and barrierless way, contrary to N-doped CACs, where a free-energy barrier of  $\sim 5$  kcal/mol is required to cleave the C–O bond in the C–O–H adduct.<sup>10</sup> The difference arises presumably from the fact that the B–O bond is somewhat weaker than the C–O bond; therefore, the formation of a metastable intermediate observed for N-doped CACs is avoided. Hence, a complete reduction of  $\text{O}_2$  to  $\text{H}_2\text{O}$  would occur, following the formal reaction  $\text{O}_2 + 4\text{H}^+ + 4\text{e}^- \rightarrow 2\text{H}_2\text{O}$  for the c-2 site of Figure 2. Overall, our simulations suggest that the rate-determining step for ORR on this catalytic site is the first  $\text{O}_2$  adsorption process if only the B–N-doped zigzag-edged surface is present in synthesized CACs.

Similarly, a  $\text{H}^+$  attack to the terminal O of an adsorbed  $\text{O}_2$  occurs selectively for the zigzag-shaped step edge. Contrary to the zigzag-edged surface, both O atoms in the resulting  $-\text{B}-\text{O}-\text{O}-\text{H}$  adduct at the step edge are readily accessible to an additional  $\text{H}^+$  because of the absence of nearby hydrophobic groups facing water (see Figures 4b and 5c). Thus, the reaction path is bifurcated just after the conversion to the  $-\text{B}-\text{O}-\text{O}-\text{H}$  adduct. In the first path, by adding two extra electrons and one extra proton in the order of  $\text{e}^-$ ,  $\text{H}^+$ , and  $\text{e}^-$ , the B–O bond in the  $-\text{B}-\text{O}-\text{O}-\text{H}$  adduct is cleaved upon a  $\text{H}^+$  attack to the O atom bound to B, resulting in an undesired final product,  $\text{H}_2\text{O}_2$ , as shown in Figure 5c. Therefore, the reduction of  $\text{O}_2$  in this path can be summarized as  $\text{O}_2 + 2\text{H}^+ + 2\text{e}^- \rightarrow \text{H}_2\text{O}_2$ . On the other hand, the second path is similar to the one described above for the zigzag-edged surface, apart from the presence of an activation barrier characterizing the third proton-transfer step. By adding additional electrons and protons according to the sequence,  $\text{e}^-$ ,  $\text{e}^-$ , and  $\text{H}^+$ , the O–O bond in the  $-\text{B}-\text{O}-\text{O}-\text{H}$  adduct breaks upon a  $\text{H}^+$  attack to the terminal O, leading to the formation of the first  $\text{H}_2\text{O}$ . We then observed that the remaining O on the adsorption site reverts immediately into a slightly stable intermediate by the cleavage of the B–C bond and simultaneous formation of a new C–O bond, as shown in Figure 5d. Consequently, the next reduction step of the remaining adsorbed O occurs by overcoming a free-energy barrier of about 3 kcal/mol, which is comparable to that for the  $\text{O}_2$  adsorption process, according to our blue moon ensemble estimations.

## Conclusions

Our first-principles simulations show that the codoping of boron and nitrogen in CACs is an effective way to further enhance their catalytic activity, at least in two respects. First, strong attractive interatomic interaction between neighboring B and N will help N dopants to occupy a particular site suitable for enhancing the catalytic activity of CACs. Second, the B–N codoping is able to activate the energetically favored dopant sites, which, in the corresponding single-dopant configurations, would be catalytically inert. Because these sites could be realized with higher probability, their activation is a key to the production of catalytically efficient CACs. Moreover, free-energy barriers would be remarkably reduced for both  $\text{O}_2$  adsorption and subsequent reduction processes, indicating that the overall reaction rate for ORR could be significantly improved. In fact, Ozaki et al.<sup>1,2</sup> already showed that the ORR activity of CACs is enhanced by the coexistence of N and B, which is qualitatively consistent with the present work. More systematic investigations for the synthesis of BN-doped CACs are now underway and will be reported in forthcoming publications.

**Acknowledgment.** This work was partially supported by the New Energy and Industrial Technology Development Organization (NEDO). Computations were done at the JAEA Supercomputer Facility, Center for Information Science of JAIST, High Performance Computing System of Hokkaido University, and HPC resources of CCRI/CINES/IDRIS under the allocation 2009-x2009096092 by GENCI.

## References and Notes

- (1) Ozaki, J.; Kimura, N.; Anahara, T.; Oya, A. *Carbon* **2007**, *45*, 1847.
- (2) Ozaki, J.; Anahara, T.; Kimura, N.; Oya, A. *Carbon* **2006**, *44*, 3358.
- (3) Ozaki, J.; Tanifugi, S.; Kimura, N.; Furuichi, A.; Oya, A. *Carbon* **2006**, *44*, 1324.
- (4) Matter, P. H.; Wang, E.; Arisia, M.; Biddinger, E. J.; Ozkan, U. S. *J. Mol. Catal. A: Chem.* **2007**, *264*, 73.
- (5) Sidik, R. A.; Anderson, A. B.; Subramanian, N. P.; Kumaraguru, P.; Popov, B. N. *J. Phys. Chem. B* **2006**, *110*, 1787.
- (6) Maldonado, S.; Stevenson, K. *J. J. Phys. Chem. B* **2005**, *109*, 4707.
- (7) Shao, Y.; Sui, J.; Yin, G.; Gao, Y. *Appl. Catal., B* **2008**, *79*, 89.
- (8) Tanabe, Y.; Yasuda, E. *Carbon* **2000**, *38*, 329.
- (9) Niwa, H.; Horiba, K.; Harada, Y.; Oshima, M.; Ikeda, T.; Terakura, K.; Ozaki, J.; Miyata, S. *J. Power Sources* **2009**, *187*, 93.
- (10) Ikeda, T.; Boero, M.; Huang, S. F.; Terakura, K.; Oshima, M.; Ozaki, J. *J. Phys. Chem. C* **2008**, *112*, 14706.
- (11) Huang, S. F.; Terakura, K.; Ozaki, T.; Ikeda, T.; Boero, M.; Oshima, M.; Ozaki, J.; Miyata, S. *Phys. Rev. B* **2009**, *80*, 235410.
- (12) Car, R.; Parrinello, M. *Phys. Rev. Lett.* **1985**, *55*, 2471.
- (13) CPMD; IBM Corp., Zurich, Switzerland, 1990–2006; MPI für Festkörperforschung Stuttgart: Stuttgart, Germany, 1997–2001; <http://www.cpmd.org>.
- (14) Hamprecht, F. A.; Cohen, A. J.; Tozer, D. J.; Handy, N. J. *J. Chem. Phys.* **1998**, *109*, 6264.
- (15) Boese, A. D.; Doltisini, N. L.; Handy, N. C.; Sprik, M. *J. Chem. Phys.* **2000**, *112*, 1670.
- (16) Doltisini, N. L.; Sprik, M. *Phys. Chem. Chem. Phys.* **2003**, *5*, 2612.
- (17) Boero, M.; Tateno, M.; Terakura, K.; Oshiyama, A. *J. Chem. Theory Comput.* **2005**, *1*, 925.
- (18) Ikeda, T.; Boero, M.; Terakura, K. *J. Chem. Phys.* **2007**, *127*, 074503.
- (19) Ikeda, T.; Boero, M.; Terakura, K. *J. Chem. Phys.* **2007**, *126*, 034501.
- (20) Ikeda, T.; Katayama, Y.; Saitoh, H.; Aoki, K. *J. Chem. Phys.* **2010**, *132*, 121102.
- (21) Troullier, N.; Martins, J. L. *Phys. Rev. B* **1991**, *43*, 1993.
- (22) Sprik, M.; Hutter, J.; Parrinello, M. *J. Chem. Phys.* **1996**, *105*, 1142.
- (23) Wilhelm, F.; Schmickler, W.; Nazmutdinov, R. R.; Spohr, E. *J. Phys. Chem. C* **2008**, *112*, 10814.
- (24) Sprik, M.; Cicotti, G. *J. Chem. Phys.* **1998**, *109*, 7737.
- (25) Sprik, M. *Chem. Phys.* **2000**, *258*, 139.
- (26) Boero, M.; Parrinello, M.; Terakura, K. *J. Am. Chem. Soc.* **1998**, *120*, 2746.
- (27) Johnson, B. G.; Gill, P. M. W.; Pople, J. A. *J. Chem. Phys.* **1993**, *98*, 5612.
- (28) Jiang, D.; Sumpter, B. G.; Dai, S. *J. Chem. Phys.* **2007**, *126*, 134701.
- (29) Grimme, S. *J. Comput. Chem.* **2006**, *27*, 1787.

JP100045E